Nonlinear Analysis of an Injection-Locked Oscillator Coupled to an External Resonator

Víctor Ardila, *Student Member, IEEE*, Franco Ramírez, *Senior Member, IEEE*, and Almudena Suárez, *Fellow, IEEE*

***Abstract*— This work investigates an injection-locked power oscillator inductively coupled to an external resonator for wireless power transfer. The system allows a high transfer efficiency, while ensuring a constant oscillation frequency versus the coupling factor, unlike free-running implementations. An analytical formulation provides insight into the impact of the coupling factor on the locked-operation ranges. Two types of qualitative behavior, delimited by a codimension-two bifurcation, are distinguished. The investigation is extended to a Class-E oscillator at 13.56 MHz, analyzed with a new harmonic balance (HB) method that provides the family of locked-solution curves in a single simulation. Very good agreement is obtained with the measurement results.**

***Index Terms*— Bifurcation, inductive coupling, injection locking, oscillator.**

I. Introduction

NEAR-FIELD wireless power transfer is used for the short-distance recharge of sensor networks, electrical car batteries, implantable devices, and other systems [1]–[3]. A high-power oscillator [4]–[6] inductively coupled to an external resonator enables a high transmission efficiency with no need for a driving source. However, the frequency is self-generated so it will change with the operation conditions [7] and, thus, with the coupling factor k, which depends on the coil distance and misalignment [8]–[10]. Even if the standalone oscillator is suitably designed to comply with regulations, the coupling effects can make the circuit operate outside the allowed frequency band.

In this work, the undesired frequency variation will be prevented through the injection locking of the inductively coupled oscillator, investigated here for the first time to our knowledge. The oscillation frequency agrees with that of the injection source while still providing high output power from the circuit oscillation and, as a result, a very high gain [11]. Moreover, the locking can prevent the oscillation extinction under strong coupling effects, observed in free-running operation [5]. The low phase noise enabled by the locking to a source of higher spectral purity would be beneficial for data transmission, which can be carried out through phase modulation. The investigation will depart from an analytical study of the global oscillator behavior versus the coupling factor k and input signal amplitude. As will be shown, a codimension (CD)-two bifurcation [12] gives rise to two different kinds of qualitative response versus k when varying the input amplitude. The possibility of enlarging the locking range through a suitable variation of the external resonator values will also be demonstrated. The investigation will be extended to a Class-E oscillator at 13.56 MHz, analyzed with a new harmonic balance (HB) method that provides the family of locked-solution curves in a single simulation. Its locking range will be enlarged with the aid of the new criteria. The analysis results will be validated with measurements.

Manuscript received February 24, 2022; revised March 17, 2022; accepted March 20, 2022. This work was supported by the Spanish Ministry of Science and Innovation and the European Regional Development Fund (MCIN/AEI/10.13039/501100011033/ERDF "A way of making Europe") under Grant TEC2017-88242-C3-1-R and Grant PID2020-116569RB-C31. *(Corresponding author: Franco Ramírez.)*

The authors are with the Departamento de Ingeniería de Comunicaciones, Universidad de Cantabria, Santander, Spain (e-mail: victorangel.ardila@unican.es; ramirezf@unican.es; almudena.suarez@unican.es).

This article was presented at the IEEE MTT-S International Microwave Symposium (IMS 2022), Denver, CO, USA, June 19–24, 2022.

Color versions of one or more figures in this letter are available at https://doi.org/10.1109/LMWC.2022.3163605.

Digital Object Identifier 10.1109/LMWC.2022.3163605

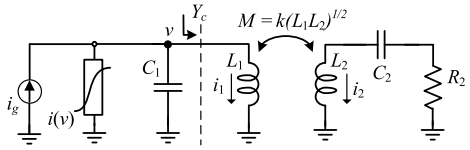

Fig. 1. Simple oscillator used in the analytical study: $C_1 = C_2 = 53$ pF; $L_1 = L_2 = 2.6$ μH; $R_2 = 50$ Ω; and $i(v) = av + bv^3$ ($a = -0.01$ A/V and $b = 0.01$ A/V^3).

II. Analytical Study

The analytical study will be based on the simple cubic nonlinearity oscillator shown in Fig. 1. We will assume an oscillation locked to the injection current source of amplitude I_g at the frequency ω. Performing the analysis at the fundamental frequency, one obtains

$$\left[G_T(V) + jC_1\omega + \left(jL_1\omega + \frac{jk^2L_1L_2C_2\omega^3}{1 - L_2C_2\omega^2 + jR_2C_2\omega}\right)^{-1}\right] V = I_g e^{j\phi} \quad (1)$$

where V is the voltage amplitude, $G_T(V) = a + \beta V^2$ is the describing function of the active device having $a < 0$ and $\beta > 0$, ϕ is the opposite of the phase shift between the node voltage and the input current, k is the coupling factor, and the other various elements are described in the caption of Fig. 1.

A case of particular interest is the injection locking at the central frequency ω_o of the allowed operation band. To maximize the power transfer, we will also impose $\omega_o = 2\pi f_o = 1/(L_1C_1)^{1/2} = 1/(L_2C_2)^{1/2}$ under the usual condition $L_1 = L_2 = L$, so $C_1 = C_2 = C$. Thus, ω_o agrees with the free-running frequency. Particularizing (1) to this case and splitting the equation into real and imaginary parts,

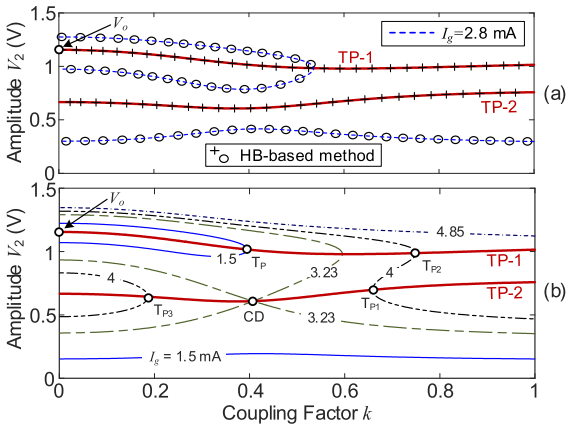

Fig. 2. Solution curves in terms of V versus k with the turning point loci (in red) superimposed. (a) $I_g = 2.8$ mA. (b) Curve family when varying I_g.

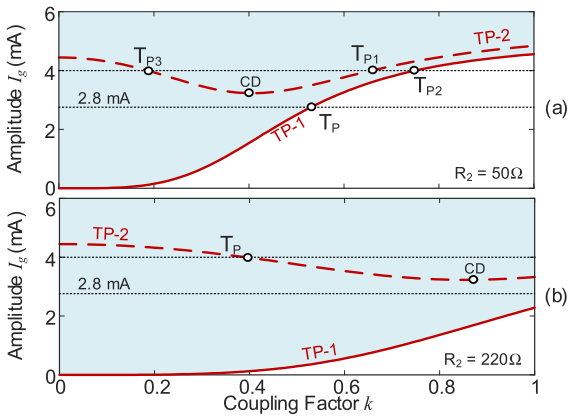

Fig. 3. Turning point loci in the plane defined by k and I_g. The locked-operation region is shadowed. (a) $R_2 = 50\ \Omega$. (b) $R_2 = 220\ \Omega$.

one obtains

$$H_{T,r}(V) = H_r(V) - I_g \cos\phi = 0 \quad (2a)$$
$$H_{T,i}(V) = H_i(V) - I_g \sin\phi = 0 \quad (2b)$$

where

$$H_r(V) = aV + \beta V^3 + k^2 V\left[R_2 + k^4 L/(CR_2)\right]^{-1} \quad (3a)$$
$$H_i(V) = C\omega_o V - V\left[L\omega_o + k^4 L^2 \omega_o/(CR_2^2)\right]^{-1}. \quad (3b)$$

To obtain the curve providing V at ω_o versus k at a given I_g, we will square and add the terms in (3a) and (3b)

$$H_r^2(V) + H_i^2(V) = I_g^2. \quad (4)$$

For each k, one has a bicubic equation in V^2. For small I_g, there will be three solutions up to a certain k. This is shown in Fig. 2(a), where the solutions of (4) are traced versus k (dashed curves) for $I_g = 2.8$ mA. The results are validated with HB. The oscillation is excited only in the higher amplitude curve. In the isolated open curve, the circuit responds to the injection signal in a nonautonomous manner. To get some insight, one can consider a low I_g and approach the two higher amplitude solutions at $k = 0$ by linearizing (4) about the free-running amplitude V_o, which provides $V = V_o \pm I_g/(a + 3\beta V_o^2)$. For low I_g, the oscillation curve [Fig. 2(a)] would depart from two points symmetrically located above and below V_o, with a larger amplitude difference for a higher I_g.

For a general analysis versus I_g, we will return to the nonlinear system (2a). As seen in Fig. 2(a), the locked-operation interval is delimited by a turning point in the high amplitude curve. At turning points, the system Jacobian matrix becomes singular [12], [13], which in (2a) (as easily derived) leads to

$$\det\begin{bmatrix} \partial H_{T,r}/\partial V & \partial H_{T,r}/\partial \phi \\ \partial H_{T,i}/\partial V & \partial H_{T,i}/\partial \phi \end{bmatrix} = \frac{\partial H_r^2}{\partial V} + \frac{\partial H_i^2}{\partial V} = 0. \quad (5)$$

This provides an explicit expression for V at the turning points of the injection-locked coupled oscillator

$$V_T^2 = \left(-2(a+A) \pm \sqrt{(a+A)^2 - 3B^2}\right)/(3\beta) \quad (6)$$

where

$$A = k^2\left(k^4 \frac{L}{CR_2} + R_2\right)^{-1}$$
$$B = C\omega_o - \omega_o^{-1}\left(L + \frac{L^2}{CR_2^2}k^4\right)^{-1}. \quad (7)$$

Applying (5)–(7) to the circuit shown in Fig. 1, one obtains the loci traced by the solid red lines in Fig. 2(a). Note that I_g varies through the loci and the solution curves are for $I_g = 2.8$ mA. The crossing with the upper turning point locus (TP-1) provides maximum k up to which the system remains locked. The family of locked curves when varying I_g is shown in Fig. 2(b). Again, the turning point loci are traced in solid red lines. One obtains two kinds of qualitative behavior. For low I_g, there is a locked-solution curve with a turning point and a low-amplitude open curve. Then, there is a CD-two bifurcation [12] at which the two curves merge. For larger I_g, the higher amplitude becomes open and exhibits two turning points (T_{P1} and T_{P2}). In turn, the lower amplitude exhibits a turning point (T_{P3}), and so it does not exist for all k. The turning points T_{P2} and T_{P3} are a result of the system continuity and originate from the curve splitting after CD. When further increasing I_g, the lower amplitude curve shrinks and eventually vanishes, and the higher amplitude curve does not exhibit any turning points. In view of the impact of I_g on the k interval in locked conditions, it will be useful to trace the tuning-point loci in the plane defined by k and I_g. This is done by sweeping k and, at each k step, obtaining V_T from (6) and replacing the resulting V_T values in (4), which is compactly written as

$$\left[a + A + \beta V_T^2\right]^2 V_T^2 + B^2 V_T^2 = I_g^2. \quad (8)$$

Fig. 3 shows the two loci in the plane k, I_g, indicated as TP-1 and TP-2, respectively; locked solutions are obtained in the shadowed regions. As expected, the loci start from the same values at $k = 0$, when the circuit is isolated from the resonator. The lower turning point locus (TP-1) provides the maximum k in locked conditions. The higher turning point locus (TP-2), denoted by a dashed line, exhibits a minimum at CD. The section of TP-2 on the left of CD provides the turning point in the low-amplitude curve generated after the merging. The section on the right of CD provides, together with TP-1, a multivalued section in the open solution curve. Besides (6) and (8), CD fulfills $\partial I_g/\partial k = 0$ since it is an extreme of TP-2 in the plane defined by k and I_g. To maximize the locking range at a given I_g, one should limit the impact of k on (4). This can be achieved by reducing both A and B through the increase in R_2. Fig. 3 shows a comparison of the loci obtained for $R_2 = 50\ \Omega$ and $R_2 = 220\ \Omega$ is shown in Fig. 3(b).

III. Injection-Locked FET-Based Oscillator

A. Oscillator Design

The Class-E oscillator is shown in Fig. 4(a) and the measurement set-up is shown in Fig. 4(b). Initially, we design a Class-E amplifier at $f_o = 13.56$ MHz, excited with the

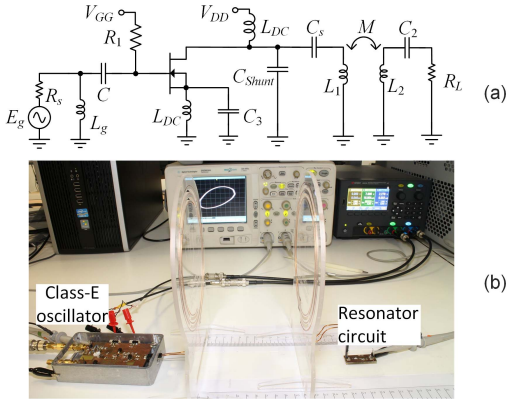

Fig. 4. Class-E oscillator based on the transistor IRLML0040TRPbF (FR-4 substrate). (a) Schematic. $R_1 = 1.5$ kΩ, $L_g = 70$ nH, $L_S = 0.1$ μH, $L_{dc} = 15$ μH, $L_1 = L_2 = 2.8$ μH, $C = 33$ nF, $C_3 = 5.6$ nF, $C_{Shunt} = 20$ pF, $C_S = 75$ pF, and $C_2 = 55$ pF. (b) Experimental setup. Coils (AWG 18 copper wire) mounted on support machines using acrylic plastic sheets.

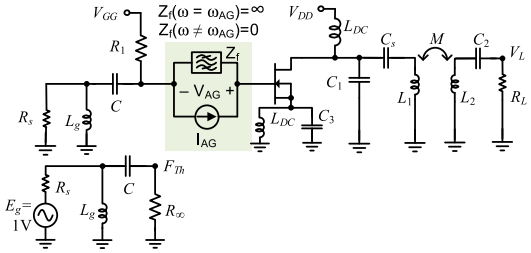

Fig. 5. Analysis through the simultaneous simulation of two circuits.

amplitude V_g. It is terminated with a coupled resonator, considering the intermediate factor $k = 0.2$. We set $R_2 = 50\ \Omega$ and calculate L_1, C_s, and C_1 for a Class-E operation. To get an oscillator [7], we introduce an ideal reactive feedback $\Gamma = 0.99e^{j\theta}$ in series at the source terminal and select the θ value providing the largest negative conductance when looking into the transistor gate. Here, it corresponds to a capacitor (C_3). Next, we connect an auxiliary generator (AG) at ω_o [8]–[10] at the gate terminal with the amplitude $V_{AG} = V_g$ to obtain the admittance function $Y_N(V_g, \omega_o)$. Then, we calculate the input network to fulfill $Y_T(V_g, \omega_o) = Y_{in}(\omega_o) + Y_N(V_g, \omega_o) = 0$, which, in this case, corresponds to an inductor in parallel with a resistor.

B. Oscillator Analysis

The HB analysis is carried out with a novel method based on the simultaneous simulation of two circuits (Fig. 5). The first circuit corresponds to the oscillator in the absence of the input source. It is used to obtain a nonlinear admittance/impedance function (calculated by means of an AG [14]) that describes the complete oscillator circuit from the observation node/branch. The second circuit is used to obtain the Norton/Thevenin equivalent of the input network (up to the AG location [14]). In the case of the driven oscillator shown in Fig. 4, a Thevenin equivalent is considered, so a current AG is chosen. It is connected in series at the device input branch and operates at the frequency ω_o with an ideal bandpass filter in parallel (Fig. 5). One performs a double sweep in k and the AG current amplitude I_{AG} and uses the first circuit to calculate $Z_T(k, I_{AG}) = V_{AG}/I_{AG}$, where V_{AG} is the voltage drop across the AG. The lower circuit (Fig. 5) is used to calculate

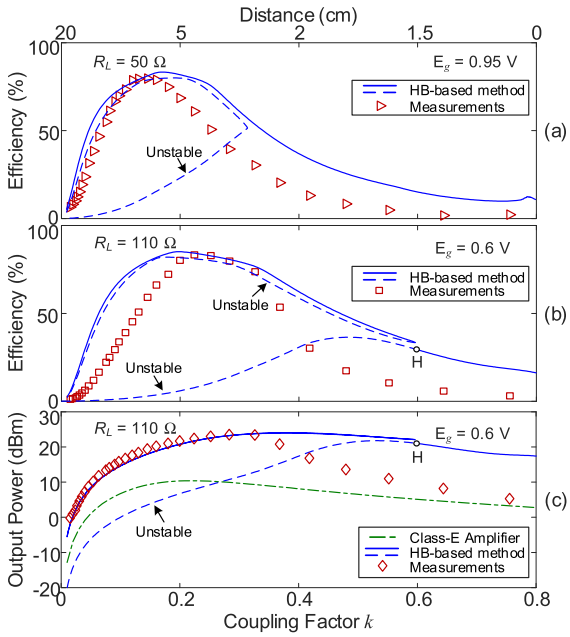

Fig. 6. Solution curves. Stable sections are traced as solid line. Measurements are superimposed. (a) Efficiency for $E_g = 0.95$ V and $R_L = 50\ \Omega$. (b) Efficiency for $E_g = 0.6$ V and $R_L = 110\ \Omega$. (c) Output power for $E_g = 0.6$ V and $R_L = 110\ \Omega$.

the Thevenin voltage V_{Th} and should be terminated in an open circuit (an ideally infinite resistor R_∞ is introduced, for generality). This circuit is excited with a dummy source of value $E_g = 1$ V and the resulting open-circuit voltage is F_{Th}, which agrees with the linear voltage ratio $F_{Th} = V_{Th}/E_g$. Combining V_{Th} with $Z_T(k, I_{AG})$, the solution curves versus k will correspond to the contour levels in $|E_g|$ of the function

$$|Z_T(k, I_{AG})|I_{AG}/|F_{Th}| = |E_g|. \tag{9}$$

Note that commercial HB does not provide by default any injection-locked solutions [15]. The efficiency and output power are obtained by interpolating the dc power and load-voltage amplitude V_L through the curves (9). Fig. 6(a) shows the efficiency for $E_g = 0.95$ V and $R_L = 50\ \Omega$, just after the CD-two bifurcation. Stable locked solutions (solid line) are obtained for the whole k range. Measurements for distances $d = 0.5$ cm to $d = 20$ cm are superimposed. Discrepancies are attributed to inaccuracies in k estimation. According to the analytical derivations, a higher R_L should reduce the input power required to keep the system locked at all k. See the efficiency and output power for $E_g = 0.6$ V and $R_L = 110\ \Omega$ in Fig. 6(b) and (c). The system operates just before the CD-two bifurcation and the low amplitude curve becomes stable through an inverse Hopf bifurcation (H) [12]. The system transfers up to 24 dBm with $P_{in} = -0.46$ dBm. As expected, the transferred power for $P_{in} = -0.46$ dBm in a Class-E amplifier (based on the same device and output network) is much lower.

IV. Conclusion

An investigation of an injection-locked oscillator coupled to an external resonator has been presented. It demonstrates two different qualitative behaviors versus the coupling factor, depending on the input amplitude. A criterion to enlarge the locked-operation intervals has also been derived. The methods have been applied to a Class-E oscillator at 13.56 MHz.

REFERENCES

[1] J. Garnica, R. A. Chinga, and J. Lin, "Wireless power transmission: From far field to near field," *Proc. IEEE*, vol. 101, no. 6, pp. 1321–1331, Jun. 2013.

[2] S. R. Khan, S. K. Pavuluri, and M. P. Y. Desmulliez, "Accurate modeling of coil inductance for near-field wireless power transfer," *IEEE Trans. Microw. Theory Techn.*, vol. 66, no. 9, pp. 4158–4169, Sep. 2018.

[3] W.-T. Chen, R. A. Chinga, S. Yoshida, J. Lin, and C.-K. Hsu, "A 36 W wireless power transfer system with 82% efficiency for LED lighting applications," *Trans. Jpn. Inst. Electron. Packag.*, vol. 6, no. 1, pp. 32–37, 2013.

[4] Q. Ma, M. R. Haider, S. Yuan, and S. K. Islam, "Power-oscillator based high efficiency inductive power-link for transcutaneous power transmission," in *Proc. 53rd IEEE Int. Midwest Symp. Circuits Syst.*, Aug. 2010, pp. 537–540.

[5] A. Jarndal and T. Petrovic, "GaN-based oscillators for wireless power transfer applications," in *Proc. Int. Conf. Adv. Comput. Telecommun. (ICACAT)*, Dec. 2018, pp. 1–5.

[6] Q. Ma, M. R. Haider, and S. K. Islam, "A high efficiency inductive power link and backward telemetry for biomedical applications," in *Proc. IEEE Sensors*, Nov. 2010, pp. 89–93.

[7] V. Ardila, F. Ramirez, and A. Suarez, "Nonlinear analysis of a high-power oscillator inductively coupled to an external resonator," *IEEE Microw. Wireless Compon. Lett.*, vol. 31, no. 6, pp. 737–740, Jun. 2021.

[8] O. Abdelatty, X. Wang, and A. Mortazawi, "Position-insensitive wireless power transfer based on nonlinear resonant circuits," *IEEE Trans. Microw. Theory Techn.*, vol. 67, no. 9, pp. 3844–3855, Sep. 2019.

[9] X. Wang and A. Mortazawi, "Bandwidth enhancement of RF resonators using duffing nonlinear resonance for wireless power applications," *IEEE Trans. Microw. Theory Techn.*, vol. 64, no. 11, pp. 3695–3702, Nov. 2016.

[10] O. Abdelatty, X. Wang, and A. Mortazawi, "Nonlinear resonant circuits for coupling-insensitive wireless power transfer circuits," in *IEEE MTT-S Int. Microw. Symp. Dig.*, Jun. 2018, pp. 976–979.

[11] Y. Yabe *et al.*, "Locking range maximization in injection-locked class-E oscillator—A case study for optimizing synchronizability," *IEEE Trans. Circuits Syst. I, Reg. Papers*, vol. 67, no. 5, pp. 1762–1774, May 2020.

[12] J. Guckenheimer and P. J. Holmes, *Nonlinear Oscillations, Dynamical Systems, and Bifurcations of Vector Fields*. New York, NY, USA: Springer, 1983.

[13] A. Suarez, "Check the stability: Stability analysis methods for microwave circuits," *IEEE Microw. Mag.*, vol. 16, no. 5, pp. 69–90, Jun. 2015.

[14] V. Ardila, F. Ramirez, and A. Suarez, "Analytical and numerical bifurcation analysis of circuits based on nonlinear resonators," *IEEE Trans. Microw. Theory Techn.*, vol. 69, no. 10, pp. 4392–4405, Oct. 2021.

[15] J. D. Cos and A. Suárez, "Efficient simulation of solution curves and bifurcation loci in injection-locked oscillators," *IEEE Trans. Microw. Theory Techn.*, vol. 63, no. 1, pp. 181–197, Jan. 2015.